

Efficient UAV Coverage in Large Convex Quadrilateral Areas with Elliptical Footprints

Alexander Vavoulas, Konstantinos K. Delibasis, Harilaos G. Sandalidis, George Nousias, and Nicholas Vaiopoulos

Abstract

Unmanned Aerial Vehicles (UAVs) have gained significant attention for improving wireless communication, especially in emergencies or as a complement to existing cellular infrastructure. This letter addresses the problem of efficiently covering a large convex quadrilateral using multiple UAVs, where each UAV generates elliptical coverage footprints based on its altitude and antenna tilt. The challenge is approached using circle-packing techniques within a unit square to arrange UAVs in an optimal configuration. Subsequently, a homography transformation is applied to map the unit square onto the quadrilateral area, ensuring that the UAVs' elliptical footprints cover the entire region. Numerical simulations demonstrate the effectiveness of the proposed method, providing insight into coverage density and optimal altitude configurations for different placement scenarios. The results highlight the scalability and potential for improving UAV-based communication systems, focusing on maximizing coverage efficiency in large areas with irregular shapes.

Index Terms

Unmanned aerial vehicles (UAVs), coverage optimization, convex quadrilaterals, ellipse packing, homography transformation, wireless communications

I. INTRODUCTION

Unmanned aerial vehicles (UAVs) can serve as airborne mobile terminals to ensure wireless connectivity during emergencies when cellular networks are unavailable or support terrestrial base stations to improve network performance [1]. Optimizing network coverage and throughput with a fixed number of UAVs presents a practical and intriguing challenge [2]. For example, in

The authors are with the Department of Computer Science and Biomedical Informatics, University of Thessaly, Papasiopoulou 2-4, 35 131, Lamia, Greece. e-mails{vavoulas,kdelimpasis,sandalidis,gnousias,nvaio}@dib.uth.gr.

[3], a mathematical model was developed to determine the optimal altitude for a single UAV to maximize its ground service area, while in [4], multi-UAV placement strategies were proposed, utilizing circle-packing techniques.

UAVs can be deployed at varying altitudes, offering increased flexibility in adapting to user distributions and terrain variations. Typically, UAVs are equipped with directional antennas with uniform half-power beamwidths (HPBWs) in both the azimuth and elevation planes, ensuring consistent gains [5]. When antennas are vertically oriented, the resulting footprints are circular. However, circular regions may not accurately reflect actual service areas in practical scenarios. For example, when antennas are tilted at angles relative to the ground's perpendicular, the resulting regions take on an elliptical shape [6]. The ability to adjust antenna orientations and UAV altitudes allows advanced solutions to optimize the balance between efficiency and resource utilization. These parameters enable dynamic network configurations that address the diverse requirements of ground users under varying environmental conditions [7].

In our previous work, we addressed the problem of determining the optimal hovering altitude for a single UAV to achieve full coverage of a convex quadrilateral region of arbitrary shape [8]. In this study, we extend the problem to scenarios where the quadrilateral region is sufficiently large, necessitating the deployment of several M UAVs to ensure adequate coverage. Specifically, we focus on covering the quadrilateral using multiple elliptical regions generated by UAVs operating at different altitudes and radiating at varying tilted angles. From a mathematical point of view, the problem is formulated as the packing of a set of arbitrary ellipses, defined by their semi-axes, within a convex polygon [9]. To solve this, we initially apply circle-packing techniques of equal-sized circles within a unit square as a foundational approach. Then, a homography transformation is utilized to map the resulting configurations onto the target quadrilateral region [10], [11].

The following introduces the homography technique that maps the enclosed circles within a unit square onto ellipses within a quadrilateral. Subsequently, a versatile path loss model is applied to determine the optimal placement of the UAVs required to cover the quadrilateral with elliptical footprints. To illustrate the methodology, a numerical example compares two scenarios with different UAV configurations.

II. HOMOGRAPHY TRANSFORMATION

We consider a convex quadrilateral Q' with vertices $P'_i = (x'_i, y'_i)$, for $i = 1, \dots, 4$. The objective is to cover Q' with M elliptical footprints generated by M UAVs. To achieve this, we first define a unit square area Q , which contains M circular disks of equal size. In the context of the circle packing problem, the goal is to arrange the M circles within the square to maximize the packing density and ensure that the circles do not overlap. The coordinates of the vertices of Q are given by $P_i = (x_i, y_i)$, for $i = 1, \dots, 4$, where $(x_1, y_1) = (0, 0)$, $(x_2, y_2) = (1, 0)$, $(x_3, y_3) = (1, 1)$, and $(x_4, y_4) = (0, 1)$. Through a homography transformation represented by the matrix \mathbf{H} the square Q is transformed into the quadrilateral Q' , as illustrated in Fig. 1 [12]

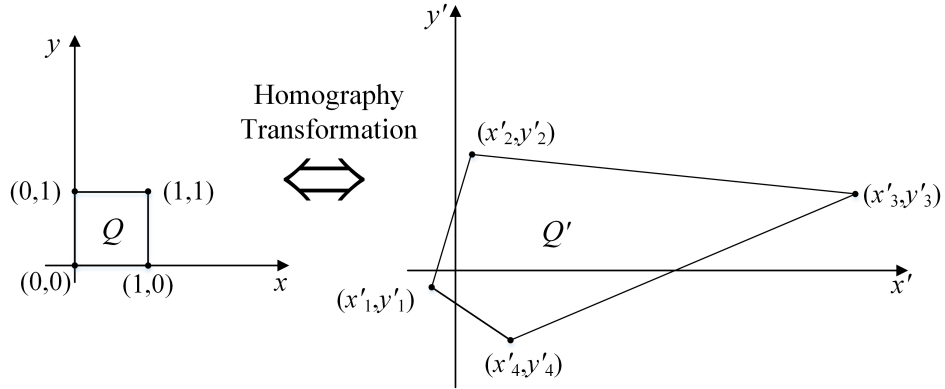


Fig. 1. Homography transformation on Q .

$$\begin{bmatrix} x' \\ y' \\ 1 \end{bmatrix} = \mathbf{H} \begin{bmatrix} x \\ y \\ 1 \end{bmatrix} = \begin{bmatrix} h_{11} & h_{12} & h_{13} \\ h_{21} & h_{22} & h_{23} \\ h_{31} & h_{32} & h_{33} \end{bmatrix} \begin{bmatrix} x \\ y \\ 1 \end{bmatrix}, \quad (1)$$

or equivalently

$$x' = \frac{h_{11}x + h_{12}y + h_{13}}{h_{31}x + h_{32}y + h_{33}}, \quad y' = \frac{h_{21}x + h_{22}y + h_{23}}{h_{31}x + h_{32}y + h_{33}}. \quad (2)$$

The elements of \mathbf{H} are determined by solving the corresponding homogeneous system of linear equations $\mathbf{B} \cdot \mathcal{H} = \mathbf{0}$, where

$$\mathcal{H}^T = [h_{11} \ h_{12} \ h_{13} \ h_{21} \ h_{22} \ h_{23} \ h_{31} \ h_{32} \ h_{33}] \quad (3)$$

and

$$\mathbf{B} = \begin{bmatrix} -x_1 & -y_1 & -1 & 0 & 0 & 0 & x'_1 x_1 & x'_1 y_1 & x'_1 \\ 0 & 0 & 0 & -x_1 & -y_1 & -1 & y'_1 x_1 & y'_1 y_1 & y'_1 \\ -x_2 & -y_2 & -1 & 0 & 0 & 0 & x'_2 x_2 & x'_2 y_2 & x'_2 \\ 0 & 0 & 0 & -x_2 & -y_2 & -1 & y'_2 x_2 & y'_2 y_2 & y'_2 \\ -x_3 & -y_3 & -1 & 0 & 0 & 0 & x'_3 x_3 & x'_3 y_3 & x'_3 \\ 0 & 0 & 0 & -x_3 & -y_3 & -1 & y'_3 x_3 & y'_3 y_3 & y'_3 \\ -x_4 & -y_4 & -1 & 0 & 0 & 0 & x'_4 x_4 & x'_4 y_4 & x'_4 \\ 0 & 0 & 0 & -x_4 & -y_4 & -1 & y'_4 x_4 & y'_4 y_4 & y'_4 \end{bmatrix}. \quad (4)$$

The matrix, \mathbf{H} , has eight degrees of freedom (DoF) since any nonzero solution to the homogeneous system can be scaled by a constant and still satisfy the system¹. Moreover, for a non-degenerate point configuration, i.e., co-linear points, \mathbf{H} is invertible since $\det(\mathbf{H}) \neq 0$. The final solution is determined by the eigenvector of $\mathbf{B}^T \mathbf{B}$ associated with the smallest nonzero eigenvalue. This solution satisfies the condition that $\sum_{ij} h_{ij}^2 = 1$.

The following presents a series of theorems that establish precise mathematical relationships between the mapping of the unit square with the enclosed circles onto the quadrilateral Q' and the ellipses within it.

Theorem 1. *The family of horizontal lines $y = y_0$ and vertical lines $x = x_0$, with x_0 and y_0 as arbitrary constants, intersect under the homography transformation \mathbf{H} at the points $\left(\frac{h_{11}}{h_{31}}, \frac{h_{21}}{h_{31}}\right)$ and $\left(\frac{h_{12}}{h_{32}}, \frac{h_{22}}{h_{32}}\right)$, respectively.*

Proof. Consider two horizontal lines in the $\{x, y\}$ plane, $y = y_i$ for $i = 1, 2$. Applying (2), we obtain

$$x' = \frac{h_{11}x + h_{12}y_i + h_{13}}{h_{31}x + h_{32}y_i + h_{33}}, \quad y' = \frac{h_{21}x + h_{22}y_i + h_{23}}{h_{31}x + h_{32}y_i + h_{33}}. \quad (5)$$

By solving the system, the corresponding equations of the lines in the $\{x', y'\}$ -plane are deduced

$$y' = \frac{h_{31}(h_{23} + h_{22}y_i) - h_{21}(h_{33} + h_{32}y_i)}{h_{31}(h_{13} + h_{12}y_i) - h_{11}(h_{33} + h_{32}y_i)} x' + \frac{h_{11}(h_{23} + h_{22}y_i) - h_{21}(h_{13} + h_{12}y_i)}{h_{11}(h_{33} + h_{32}y_i) - h_{31}(h_{13} + h_{12}y_i)}. \quad (6)$$

Eq. (6) represents a linear system 2×2 . The solution provides the intersection point of the lines in the $\{x', y'\}$ -plane. Specifically

$$\{x'_h, y'_h\} = \left\{ \frac{h_{11}}{h_{31}}, \frac{h_{21}}{h_{31}} \right\}. \quad (7)$$

¹Therefore, eight equations are sufficient to determine the nine unknown elements of \mathbf{H} .

By applying the same procedure to the parallel lines $x = x_i$ for $i = 1, 2$, we obtain the intersection point

$$\{x'_v, y'_v\} = \left\{ \frac{h_{12}}{h_{32}}, \frac{h_{22}}{h_{32}} \right\}. \quad (8)$$

□

Note that the above expressions depend solely on \mathbf{H} , regardless of x_0 , or y_0 .

Proposition 1. *A homography transformation that maps one convex quadrilateral to another is one-to-one.*

Proof. After some algebraic manipulation, the determinant of the Jacobian matrix \mathbf{J} of the homography transformation is obtained as

$$\begin{aligned} \det(\mathbf{J}) &= \frac{h_{31}(h_{12}h_{23} - h_{13}h_{22}) + h_{32}(h_{13}h_{21} - h_{11}h_{23})}{(h_{33} + h_{31}x + h_{32}y)^3} \\ &\quad + \frac{h_{33}(h_{11}h_{22} - h_{12}h_{21})}{(h_{33} + h_{31}x + h_{32}y)^3} \end{aligned} \quad (9)$$

Since the nominator does not depend on x, y , the determinant is nonzero everywhere in the $\{x, y\}$ -plane; thus, the transform is invertible and, therefore, one-to-one [13]. □

Theorem 2. *Under a homography transformation, a circle is mapped to a conic curve.*

Proof. The general form of the equation of a circle is given by [14, eq. (3.315.b)]

$$Ax^2 + Ay^2 + Dx + Ey + F = 0. \quad (10)$$

By solving (2) for x, y we get

$$x = \frac{\hat{h}_{11}x' + \hat{h}_{12}y' + \hat{h}_{13}}{\hat{h}_{31}x' + \hat{h}_{32}y' + \hat{h}_{33}}, \quad y = \frac{\hat{h}_{21}x' + \hat{h}_{22}y' + \hat{h}_{23}}{\hat{h}_{31}x' + \hat{h}_{32}y' + \hat{h}_{33}}, \quad (11)$$

where

$$\begin{aligned} \hat{h}_{11} &= h_{23}h_{32} - h_{22}h_{33}, & \hat{h}_{12} &= h_{12}h_{33} - h_{13}h_{32}, \\ \hat{h}_{13} &= h_{13}h_{22} - h_{12}h_{23}, & \hat{h}_{21} &= h_{21}h_{33} - h_{23}h_{31}, \\ \hat{h}_{22} &= h_{31}h_{13} - h_{11}h_{33}, & \hat{h}_{23} &= h_{11}h_{23} - h_{13}h_{21}, \\ \hat{h}_{31} &= h_{22}h_{31} - h_{21}h_{32}, & \hat{h}_{32} &= h_{11}h_{32} - h_{12}h_{31}, \\ \hat{h}_{33} &= h_{12}h_{21} - h_{11}h_{22}. \end{aligned}$$

Applying the transformation (11) to (10), the circle is mapped in the $\{x', y'\}$ -plane to a conic section, which is generally represented as

$$A'x'^2 + B'x'y' + C'y'^2 + D'x' + E'y' + F' = 0, \quad (12)$$

where

$$\begin{aligned} A' &= A(\hat{h}_{11}^2 + \hat{h}_{21}^2) + \hat{h}_{31}(D\hat{h}_{11} + E\hat{h}_{21}) + F\hat{h}_{31}^2, \\ B' &= \hat{h}_{11}(2A\hat{h}_{12} + D\hat{h}_{32}) + \hat{h}_{21}(2A\hat{h}_{22} + E\hat{h}_{32}) \\ &\quad + \hat{h}_{31}(D\hat{h}_{12} + E\hat{h}_{22} + 2F\hat{h}_{32}), \\ C' &= A(\hat{h}_{12}^2 + \hat{h}_{22}^2) + \hat{h}_{32}(D\hat{h}_{12} + E\hat{h}_{22}) + F\hat{h}_{32}^2, \\ D' &= \hat{h}_{11}(2A\hat{h}_{13} + D\hat{h}_{33}) + \hat{h}_{21}(2A\hat{h}_{23} + E\hat{h}_{33}) \\ &\quad + \hat{h}_{31}(D\hat{h}_{13} + E\hat{h}_{23} + 2F\hat{h}_{33}), \\ E' &= \hat{h}_{12}(2A\hat{h}_{13} + D\hat{h}_{33}) + \hat{h}_{22}(2A\hat{h}_{23} + E\hat{h}_{33}) \\ &\quad + \hat{h}_{32}(D\hat{h}_{13} + E\hat{h}_{23} + 2F\hat{h}_{33}), \\ F' &= A(\hat{h}_{13}^2 + \hat{h}_{23}^2) + \hat{h}_{33}(D\hat{h}_{13} + E\hat{h}_{23}) + F\hat{h}_{33}^2. \end{aligned}$$

The conic section is not a circle, as $A' \neq C'$, due to $\det(\mathbf{H}) \neq 0$, which implies $h_{11} \neq h_{21}$, $h_{12} \neq h_{22}$, and $h_{13} \neq h_{23}$. \square

The conditions necessary to represent an ellipse are as follows: $4A'C' - B'^2 > 0$ and $C'D'^2 + A'E'^2 - B'D'E' - 4A'C'F' + B'^2F' > 0$.

Corollary 1. *A circle transformed by a convex-to-convex homography is mapped to an ellipse.*

Proof. As stated in Proposition 1, a convex-to-convex homography is one-to-one and invertible. Specifically, the homography in question maps a square to a given quadrilateral. According to Theorem 2, a circle inscribed within the square will be transformed into a conic section that is not a circle. If the transformation results in a hyperbola or parabola, the circle intersects the quadrilateral, which leads to a contradiction. Therefore, the transformation must yield an ellipse. \square

Corollary 2. *Any two intersecting, non-intersecting, or tangent circles within the square Q are transformed by homography into conic curves that intersect, do not intersect, or are tangent, respectively.*

Proof. According to Proposition 1, the homography transformation is one-to-one. Thus, if two curves are tangent at a point, their transformed counterparts will be tangent at a single point since the transformation cannot map the common point to two separate locations. By similar reasoning, any pair of non-intersecting or intersecting curves will be mapped to non-intersecting or intersecting curves, respectively. As a result, if two touching circles share a common point inside Q , their corresponding conic sections will share the transformed point after applying the homography \mathbf{H} . \square

III. UAV PLACEMENT

In general, the optimal UAV placement is formulated as the minimization of the maximum path loss, PL_{\max} , at the boundary of the coverage region. A simplified path loss model is employed, incorporating the probability of maintaining a line-of-sight (LoS) connection, $\mathbb{P}(\text{LoS})$, influenced by the environment and UAV altitude as defined in [3]. The LoS probability is modeled using a sigmoid function with parameters η and κ . At the same time, the elevation angle at the boundary is determined by the UAV's height and the geometry of the coverage area [8]. The maximum path loss is calculated as a weighted sum of LoS and non-line-of-sight (NLoS) components

$$PL_{\max} = \mathbb{P}(\text{LoS}) \times PL_{\text{LoS}} + \mathbb{P}(\text{NLoS}) \times PL_{\text{NLoS}}, \quad (13)$$

where PL_{LoS} and PL_{NLoS} are derived from the total distance d , operating frequency f , and additional losses ξ_{LoS} , ξ_{NLoS} due to scattering and shadowing [8]. This formulation captures the impact of environmental and geometric factors on the optimization of the UAV placement.

Adopting this model for each of the M UAVs deployed to cover the quadrilateral Q' , the optimal altitude, $H_{\text{OPT},i}$ (where $i = 1, \dots, M$), can be determined to minimize the corresponding maximum path loss, $PL_{\max,i}$. Leveraging the methodology outlined in [8], a unified analytical expression for the optimal altitude of each UAV is derived as follows:

$$PL_{\max,i} = \frac{\xi_{\text{LoS}} - \xi_{\text{NLoS}}}{1 + \eta \exp \left(-\kappa \left(\arctan \left(\frac{H_i b_i}{a_i b_i + \sqrt{(b_i^2 + H_i^2)(a_i^2 - b_i^2)}} \right) - \eta \right) \right)} + 10 \log \left(H_i^2 + \left(\frac{a_i b_i + \sqrt{(b_i^2 + H_i^2)(a_i^2 - b_i^2)}}{b_i} \right)^2 \right) + 20 \log (4\pi f/c) + \xi_{\text{NLoS}}. \quad (14)$$

where $\{a_i, b_i\}$ are the major and minor semi-axes of the corresponding elliptical footprint, while H_i represents the altitude of the associated UAV and c is the speed of light. It is important

to note that the ground projection of each UAV aligns with the direction defined by the major axis of its corresponding elliptical footprint. The major and minor semi-axes, a_i and b_i , can be expressed through (12) as

$$a_i = \sqrt{\mu \frac{A'_i + C'_i + \sqrt{(A'_i - C'_i)^2 + B_i'^2}}{2}}, \quad (15)$$

$$b_i = \sqrt{\mu \frac{A'_i + C'_i - \sqrt{(A'_i - C'_i)^2 + B_i'^2}}{2}}, \quad (16)$$

where $\mu = 4\delta_1\delta_2^{-2}$, $\delta_1 = C'_iD_i'^2 + A_iE_i'^2 - B_i'D_i'E_i' - F_i'\delta_2$, $\delta_2 = 4A_i'C_i' - B_i'^2$ for $i = 1, \dots, 4$. For a given value of H_i , the tilt and semi-axis angles, ψ_i and θ_i , respectively, are expressed in terms of a_i and b_i as described in [8]

$$\psi_i = \arccos \left(\frac{\sqrt{b_i^2 H_i^2 + b_i^4}}{\sqrt{a_i^2 H_i^2 + b_i^4}} \right), \quad (17)$$

$$\theta_i = \arcsin \left(\frac{b_i^2}{\sqrt{a_i^2 H_i^2 + b_i^4}} \right). \quad (18)$$

The optimal altitude, $H_{\text{OPT},i}$, for each of the M UAVs can be found by numerically solving for the root of

$$\frac{\partial PL_{\text{max},i}}{\partial H_i} = 0. \quad (19)$$

IV. CASE STUDY

We investigate a multi-UAV network operating at a carrier frequency of 2 GHz in different environmental conditions, characterized by the parameter set $(\xi_{\text{LOS}}, \xi_{\text{NLOS}}, \eta, \kappa)$, for the following scenarios: suburban (0.1, 21, 4.88, 0.43), urban (1, 20, 9.61, 0.16), and dense urban (1.6, 23, 12.08, 0.11) [3]. A typical quadrilateral Q' is considered, preserving the shape shown in Fig. 1, with vertices at $P'_1 = (-100, -100)$, $P'_2 = (200, -300)$, $P'_3 = (1500, 250)$, and $P'_4 = (50, 400)$ in the x' - y' -plane, where all coordinates are expressed in meters. Its area can be calculated using the shoelace formula, yielding $S = 586,250\text{m}^2$ [15]. Without loss of generality, we assume a unit square Q . The homography matrix is obtained by substituting the vertices x_i, y_i

of Q and x'_i, y'_i of Q' (for $i = 1, \dots, 4$) into \mathbf{B} in (4) and solving the resulting homogeneous system, resulting in

$$\mathbf{H} = \begin{bmatrix} 0.5796 & 0.2807 & -0.2312 \\ -0.2912 & 0.6273 & -0.2312 \\ -0.0006 & -0.0013 & 0.0023 \end{bmatrix}. \quad (20)$$

We focus on two typical UAV configurations consisting of $M = 4$ and $M = 9$ UAVs. Initially, equal-sized circle packing configurations are applied to the unit square Q . These configurations are then transformed into ellipse-packing ones via the homography transformation, as depicted in Fig. 2. The selection of specific M values is determined by their ability to maximize coverage density within the range $M \in [2, 15]$ for the circle packing problem, thus optimizing the performance for the quadrilateral area considered [16]. Specifically, the total areas of the elliptical footprints are $S_4 = 443, 210, \text{m}^2$ for the 4-ellipse configuration and $S_9 = 463, 426, \text{m}^2$ for the 9-ellipse configuration [14, eq. (3.328a)], providing 75.6% and 79.0% coverage of Q' , respectively.

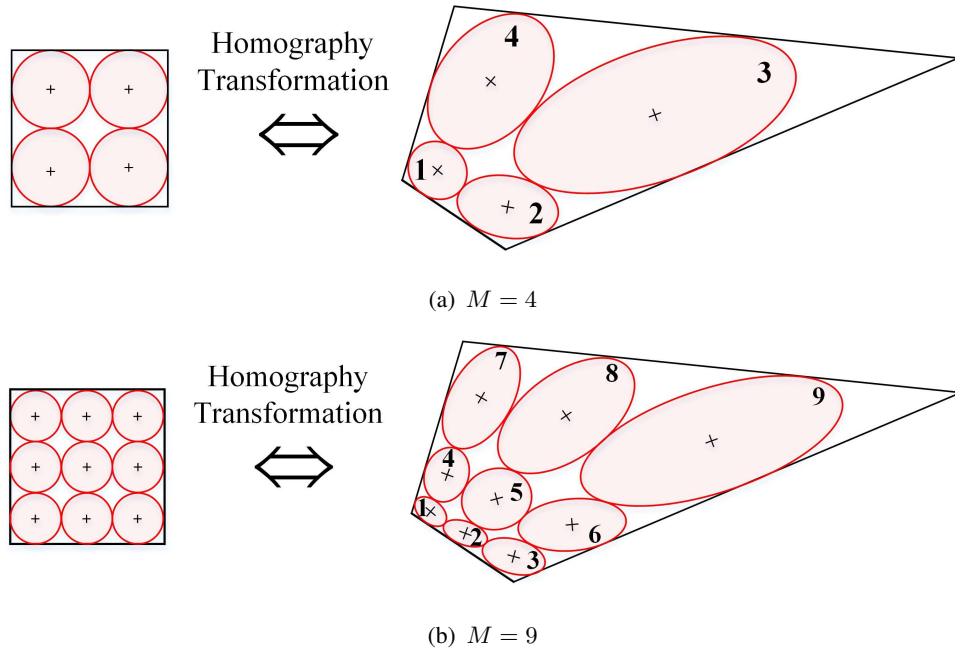


Fig. 2. Circle packing in Q vs. ellipse packing in Q'

Figures 3–5 illustrate the optimal altitudes and the corresponding maximum path losses in suburban, urban, and dense urban environments (UAV numbers align with the footprint numbers in Fig. 2). The results emphasize the flexibility of the variation in altitude between UAVs, which

facilitates more robust and adaptive network design strategies. The observed variations in PL_{max} offer valuable information to determine the transmit power requirements of each UAV, ensuring the consistent achievement of the minimum quality of service in various operating conditions.

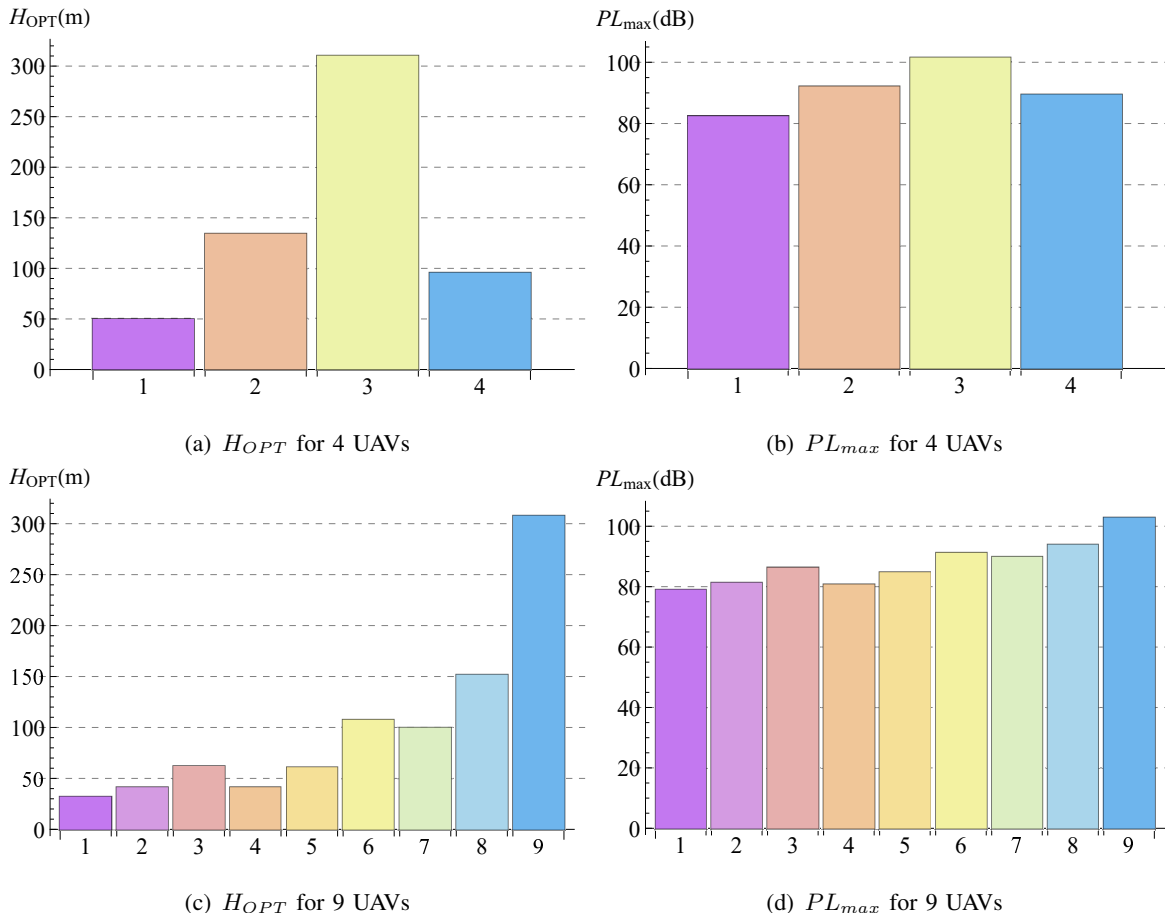


Fig. 3. Key UAV placement metrics in a suburban environment.

Finally, Fig. 6 demonstrates a detailed three-dimensional placement of the two configurations within a suburban environment. The spatial positions, tilt, and semi-apex angles of the UAVs are depicted, along with the ground footprints. Additional details regarding the exact semi-axes, optimal altitude, and angle values are included in Table I. Similar graphs can be generated for the other two environments. Such visualizations offer a comprehensive overview of the network architecture, effectively highlighting the proposed framework and the spatial characteristics of the UAV placement.

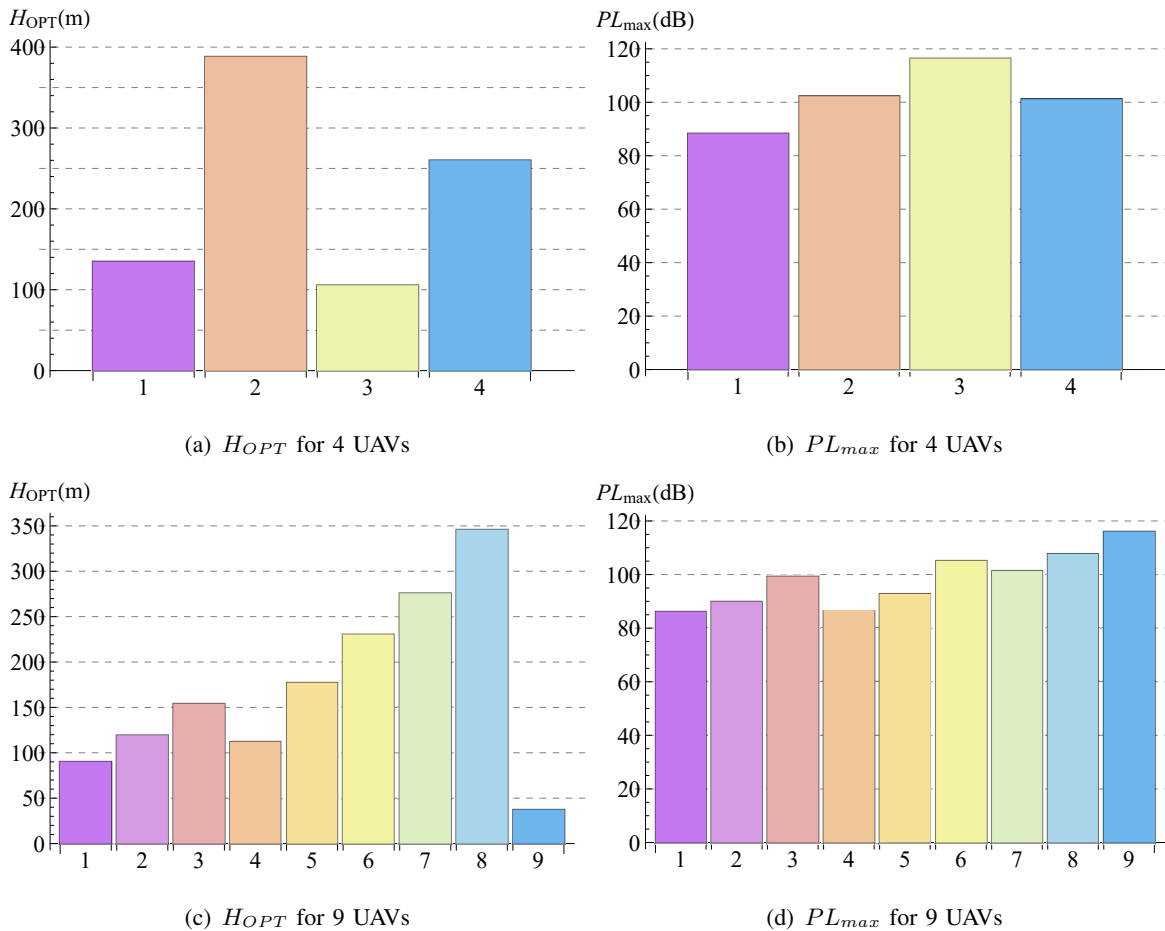


Fig. 4. Key UAV placement metrics in an urban environment.

V. CONCLUSIONS

In conclusion, the current work addresses the challenge of efficiently covering a large convex quadrilateral area using multiple UAVs that generate elliptical footprints through directional antennas. We derive an optimal UAV placement strategy by applying circle-packing techniques to a unit square and then transforming the configuration via homography to fit the quadrilateral. Through theoretical analysis and numerical simulations, we demonstrate the effectiveness of this approach in optimizing coverage and minimizing path loss. Our results indicate that the proposed method scales well with increasing UAVs and environmental conditions, offering a flexible and efficient solution for UAV-based communication systems. The derived UAV altitudes and their corresponding configurations further enhance the feasibility of real-world implementations in varying geographical and operational contexts. Future work could extend the present analysis by considering dynamic changes in the environment, user mobility, and incorporating more complex

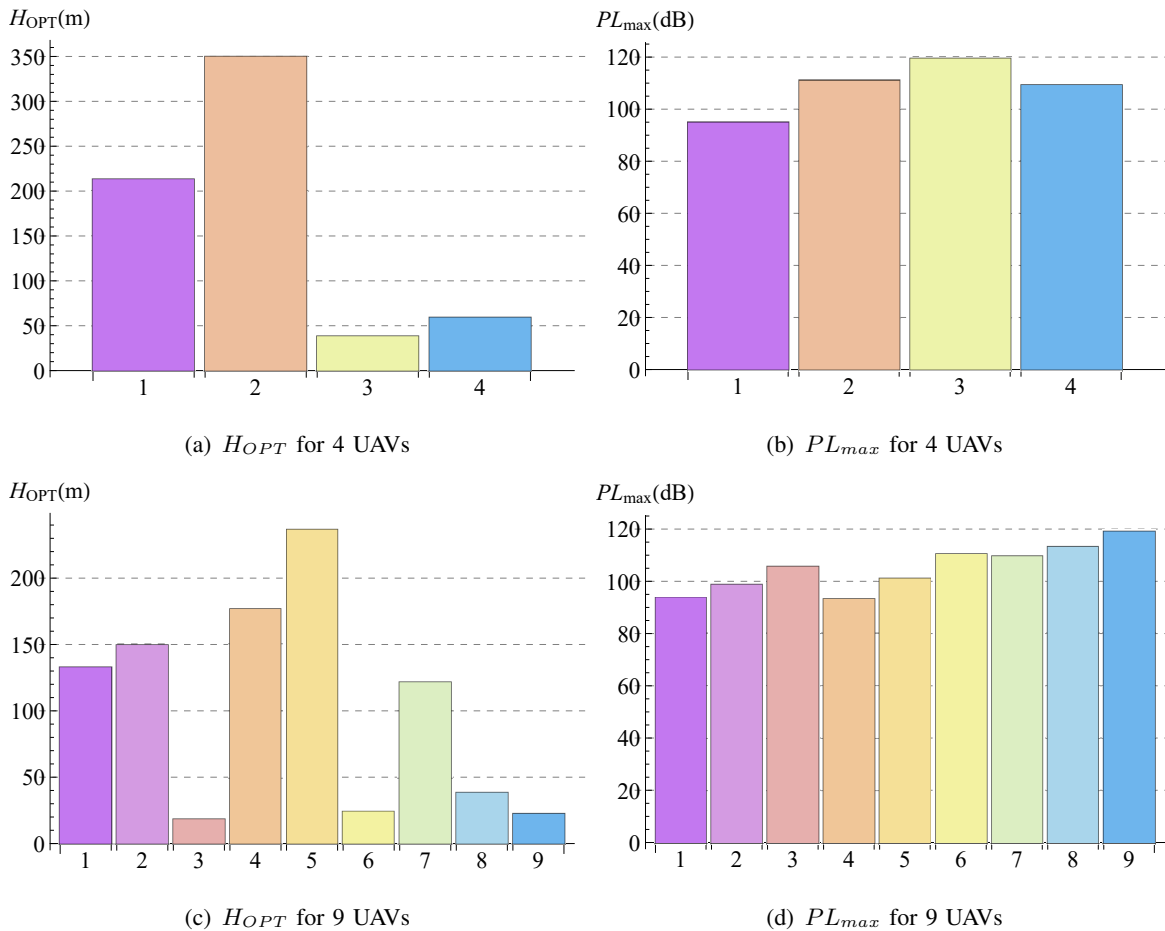
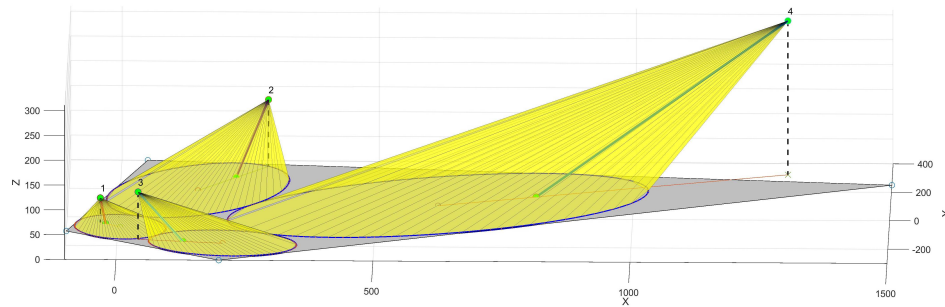


Fig. 5. Key UAV placement metrics in a dense urban environment.

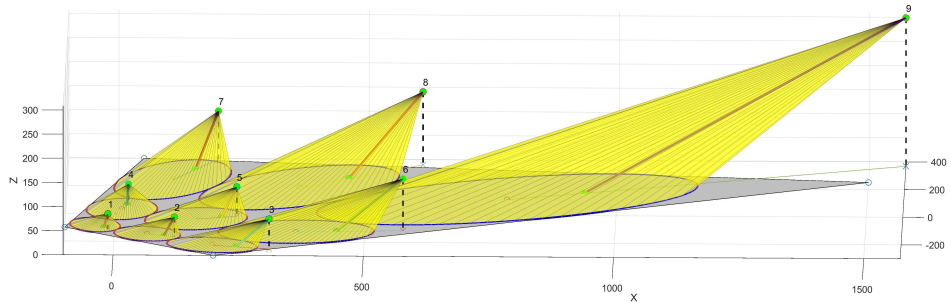
path loss models to better capture real-world conditions.

REFERENCES

- [1] N. Vaiopoulos, A. Vavoulas, and H. G. Sandalidis, "An assessment of a unmanned aerial vehicle-based broadcast scenario assuming random terrestrial user locations," *IET Optoelectron.*, vol. 15, no. 3, pp. 121–130, 2021.
- [2] M. Mozaffari, W. Saad, M. Bennis, Y.-H. Nam, and M. Debbah, "A tutorial on UAVs for wireless networks: Applications, challenges, and open problems," *IEEE Commun. Surveys Tuts.*, vol. 21, no. 3, pp. 2334–2360, 3rd Quart. 2019.
- [3] A. Al-Hourani, S. Kandeepan, and S. Lardner, "Optimal LAP altitude for maximum coverage," *IEEE Wireless Commun. Lett.*, vol. 3, no. 6, pp. 569–572, Dec. 2014.
- [4] M. Nafees, J. Thompson, and M. Safari, "Multi-tier variable height UAV networks: User coverage and throughput optimization," *IEEE Access*, vol. 9, pp. 119 684–119 699, 2021.
- [5] H. He, S. Zhang, Y. Zeng, and R. Zhang, "Joint altitude and beamwidth optimization for UAV-enabled multiuser communications," *IEEE Commun. Lett.*, vol. 22, no. 2, pp. 344–347, Feb. 2018.
- [6] A. Vavoulas, N. Vaiopoulos, H. G. Sandalidis, and K. K. Delibasis, "On the terminal location uncertainty in elliptical footprints: Application in air-to-ground links," 2023. [Online]. Available: <https://arxiv.org/abs/2309.07299>



(a) 4 UAVs



(b) 9 UAVs

Fig. 6. Key UAV placement metrics in a suburban environment.

- [7] M. M. Azari, F. Rosas, and S. Pollin, "Cellular connectivity for UAVs: Network modeling, performance analysis, and design guidelines," *IEEE Trans. Wireless Commun.*, vol. 18, no. 7, pp. 3366–3381, Jul. 2019.
- [8] A. Vavoulas, N. Vaiopoulos, K. K. Delibasis, and H. G. Sandalidis, "Optimizing coverage in convex quadrilateral regions with a single UAV," 2024. [Online]. Available: <https://arxiv.org/abs/2411.18454>
- [9] A. Pankratov, T. Romanova, and I. Litvinchev, "Packing ellipses in an optimized convex polygon," *J. Glob. Optim.*, vol. 75, no. 3, pp. 495–522, 2019.
- [10] P. G. Szabó, M. C. Markót, T. Csendes, E. Specht, L. G. Casado, and I. García, *New Approaches to Circle Packing in a Square*. New York, NY, USA: Springer-Verlag, 2007.
- [11] G. Nousias, K. Delibasis, and I. Maglogiannis, "*H*-RANSAC, an algorithmic variant for homography image transform from featureless point sets: Application to video-based football analytics," 2023. [Online]. Available: <https://arxiv.org/abs/2310.04912>
- [12] R. Hartley and A. Zisserman, *Multiple View Geometry in Computer Vision*, 2nd ed. New York, NY, USA: Cambridge Univ. Press, 2003.
- [13] W. Rudin, *Principles of Mathematical Analysis*, 3rd ed. New York, NY, USA: McGraw-Hill (Inc.), 1976.
- [14] I. N. Bronshtein, K. A. Semendyayev, G. Musiol, and H. Mühlig, *Handbook of Mathematics*, 6th ed. New York, NY, USA: Springer-Verlag, 2015.
- [15] E. W. Weisstein, "Shoelace formula," From MathWorld—A Wolfram Web Resource, 2024, accessed: 2024-11-19. [Online]. Available: <https://mathworld.wolfram.com/ShoelaceFormula.html>
- [16] Packomania, "Packomania: The circle packing problem," 2024, accessed: 2024-12-21. [Online]. Available: <http://www.packomania.com/>

TABLE I
DETAILED UAV PLACEMENT METRICS IN A SUBURBAN ENVIRONMENT

	UAV #	a_i (m)	b_i (m)	$H_{OPT,i}$ (m)	θ_i ($^\circ$)	ψ_i ($^\circ$)
4 UAVs	1	93.8	83.0	49.6	56.0	15.1
	2	217.0	146.8	134.7	36.4	36.3
	3	440.3	199.2	310.3	16.2	58.9
	4	149.2	91.9	95.7	30.6	42.7
9 UAVs	1	56.5	46.0	32.0	49.5	22.2
	2	69.5	51.8	41.4	43.0	29.2
	3	95.3	54.3	62.7	26.3	47.5
	4	78.7	70.2	41.3	56.6	14.4
	5	105.0	80.6	61.6	45.1	26.9
	6	161.3	86.4	108.0	23.2	50.9
	7	156.5	97.7	99.9	31.4	41.8
	8	228.2	125.5	151.6	24.5	49.5
	9	413.1	155.7	308.0	10.8	65.5